Journal of Catalysis 430 (2024) 115343

Contents lists available at ScienceDirect

Journal of Catalysis

journal homepage: www.elsevier.com/locate/jcat

Research article

Catalytic resonance theory: Circumfluence of programmable catalytic loops

Madeline A. Murphy [a,b], Sallye R. Gathmann [a,b], Christopher J. Bartel [b], Omar A. Abdelrahman [a,c], Paul J. Dauenhauer [a,b,*]

[a] Center for Programmable Energy Catalysis (CPEC), University of Minnesota, 421 Washington Ave. SE, Minneapolis, MN 55455, USA
[b] University of Minnesota, Department of Chemical Engineering & Materials Science, 421 Washington Ave. SE, Minneapolis, MN 55455, USA
[c] Department of Chemical Engineering, University Massachusetts Amherst, 686 N. Pleasant Street, Amherst, MA 01003, USA

ARTICLE INFO

Keywords:
Energy
Catalysis
Dynamics
Loop
Programmable

ABSTRACT

Chemical reactions on heterogeneous catalyst surfaces exhibit complex networks of elementary reactions with multiple pathways to fluid phase products, sometimes leading to surface reaction loops consisting of a closed cycle reaction pathway. While conventional catalysts at steady state exhibit zero net flux in either direction around a catalytic loop, the loop turnover frequency of three-species surface loops was evaluated in this work via microkinetic modeling to assess the reaction loop behavior resulting from a catalytic surface oscillating between two or more surface energy states. For dynamic heterogeneous catalysts undergoing applied oscillations of surface energy (i.e., programs), surface reaction loops of three species were shown to exhibit non-zero net flow of molecules around the loop, with the extent of loop turnover frequency varying with the applied frequency and amplitude of a sinusoidal or square wave oscillation. Alternatively, some dynamic surface reactions exhibited oscillations only between two surface species or resulted in surfaces covered by a single species at all times. More complex behavior was observed for dynamic surface programs of three distinct electronic states, with the temporal order of applied states controlling the direction of flow of molecules within a three-molecule surface loop. Catalytic loops have the potential to limit overall catalytic reaction rates and use energy in programmable catalysts, while some applications could purposely impose non-zero loop turnover frequency for improved surface reaction control.

1. Introduction

While heterogeneous catalytic reactions are concisely thought of as a single stoichiometric overall reaction, most surface chemistries are comprised of a network of elementary steps [1–3]. Molecules adsorb and desorb to surfaces, upon which elementary steps break and build bonds both in series and parallel. Such is the case with many critical reactions including ammonia and methanol synthesis, where N_2 or CO react with H_2 through a series of bond breaking and making steps to ultimately form NH_3 or CH_3OH, respectively [4,5]. The sequence by which hydrogen atoms form bonds with C* or N*, often on more than one catalytic site, is sufficiently complex that parallel reaction pathways exist which themselves are connected to each other [6,7]. The many options by which molecules proceed to react ultimately form reaction loops, as depicted in Fig. 1**a**, whereby molecules react and loop back on themselves (i.e., A* to B* to C* to A*) to their original state [8].

The idea of reaction loops has been considered for over a century since Onsager first examined the 'triangle reaction' in Fig. 1**b**, depicted here as a circle for inter-reacting surface species A*, B*, and C* [9]. Each surface species can react forward (e.g., A* to B*) or backward (e.g., B* to A*) with 'forward' defined herein as clockwise with forward rate constant, k_1, or reverse rate constant, k_{-1}. Reactions following mass action kinetics describe reciprocal rates forward and backward, which by the principle of microscopic reversibility highlights any microstate, being either a transition state or intermediate, is equally accessible from both the forward and reverse directions. The principle of detailed balance brings about the impossibility of a net circular reaction at equilibrium, meaning the reaction cannot take place more in one direction than the other. The principle of microscopic reversibility establishes the following reciprocal relationship for Onsager's triangle reaction,

$$1 = K_1 K_2 K_3 = \left(\frac{k_1}{k_{-1}}\right)\left(\frac{k_2}{k_{-2}}\right)\left(\frac{k_3}{k_{-3}}\right) \quad (1)$$

asserting that all elementary reactions must proceed via the same

* Corresponding author at: Center for Programmable Energy Catalysis (CPEC), University of Minnesota, 421 Washington Ave. SE, Minneapolis, MN 55455, USA.
E-mail address: hauer@umn.edu (P.J. Dauenhauer).

https://doi.org/10.1016/j.jcat.2024.115343
Received 30 September 2023; Received in revised form 28 December 2023; Accepted 24 January 2024
Available online 6 February 2024

transition state in both the forward and reverse direction [10–12]. In the case of a reaction loop, there is the possibility for two different pathways to convert A* to C* on the surface; one involving one elementary step (A*→ C*) and another involving two elementary steps (A*→ B*→ C*). In the case of a net cyclic flux, the pathway in which A* is converted to C* differs from the pathway in which C* is converted to A*. For positive flux about the reaction loop this is observed as the conversion of A* to C* proceeds via the first two elementary steps (A*→ B*→ C*), while the conversion of C* back to A* proceeds through the third (C*→ A*).

Promotion of molecules forwards or backwards along a reaction coordinate was first examined by William P. Jencks in 1969 through an oscillating enzyme mechanism [13]. Jencks theorized that an enzyme could exist in two states, E and E', such that E promoted the reverse direction with a transition state similar to the reactant(s) and E' promoted the forward reaction with a transition state similar to the product (s). This system could theoretically operate such that molecules reacting in the forward direction experience a different transition state than molecules reacting in the reverse direction, yet it avoids violations of the principle of microscopic reversibility via the switching between two distinct catalyst states [13]. In either enzyme state (E or E'), each reaction step proceeds through the same transition state such that forward and reverse rate is equal at equilibrium. Astumian and co-workers simulated the oscillating enzyme showing that energy from an external electric field switching the enzyme between states E and E' accelerates the reaction and even promotes it away from equilibrium [14,15].

Modulation of heterogeneous catalysts including metals and metal oxides between two or more states experimentally has been pursued using light, strain, or charge [16–19]. As molecules adsorb and desorb to the catalytic surface, periodic catalyst perturbations change the binding energies of the surface species as depicted in Fig. 1**c** between two or more states. The overall catalytic turnover frequency can potentially be controlled by the frequency of surface state switching with some 'resonant' frequencies exceeding the Sabatier maximum (i.e., static catalyst maximum rate) [20,21]. The *chemical* resonance conditions occur when switching between catalytic states at time scales that match the natural frequencies (e.g., first order rate constants) of each of the two slowest reaction steps [22]. For a set of conditions of applied frequency and catalyst oscillation amplitude, the energy input from external perturbations of light, strain, or charge promotes the reaction forward or backward away from equilibrium, ultimately giving each reaction a 'directionality' that does not exist in static catalytic reactions [23]. This 'kinetic asymmetry' has been defined for many dynamic systems with a ratchet structure, ultimately defining the direction of physical movement of molecular machines or reactions [24,25]. For molecular machines, the directionality can be anticipated via a non-equilibrium ratcheting constant, K_r, that predicts forward or backward bias at steady state [24,26,27]. Predictors have also been developed to assess directionality of heterogeneous catalytic reactions which also account for adsorption and desorption [21,23].

The steady state productivity of a network of elementary reactions each undergoing unique modulation associated with their chemical parameters depends on the extent of flow of molecules from reactant to product. Yet under dynamic conditions, each elementary reaction has directionality resulting from kinetic asymmetry that drives an elementary reaction forward or backward. In the triangle reaction of A* to B* to C* to A* each elementary step will have unique dynamic scaling parameters associated with that particular chemical change [23], such that different perturbations such as frequency or amplitude to the catalyst surface can flip elementary steps between forward and reverse bias. The result is that each reaction loop can consist of many different permutations of loop behavior as shown in Fig. 1**d**; some reaction loops might have all elementary steps in forward bias, while other loops might have conflicting directionality between connected elementary steps. This is further complicated when accounting for the 'strength' of each catalytic ratchet; the extent of reverse flow against the bias of the catalytic ratchet varies depending on the selected perturbation creating a 'leaky' elementary step associated with a low barrier in the reverse direction under weak binding conditions [23]. The interaction of a loop of dynamic catalytic ratchets remains to be understood for programmable heterogeneous catalysis.

Net cyclical flux in a reacting loop is undesirable with respect to energy efficiency. Modulating catalysts between states requires energy input in the form of physical forces (i.e., strain), charge, or light consistent with altering the binding energy of surface species [28]. A maximally efficient programmable catalyst achieves one mole of product per forced catalytic perturbation cycle (e.g., state 1 to state 2 to state 1) on a mole of active sites, thereby using the minimum amount of energy required to yield reaction products. Yet complex catalytic mechanisms with internal reaction loops provide a mechanism for low programmable catalyst energy efficiency; energy input to perturb the catalyst between states could be consumed to 'pump' reactions in loops

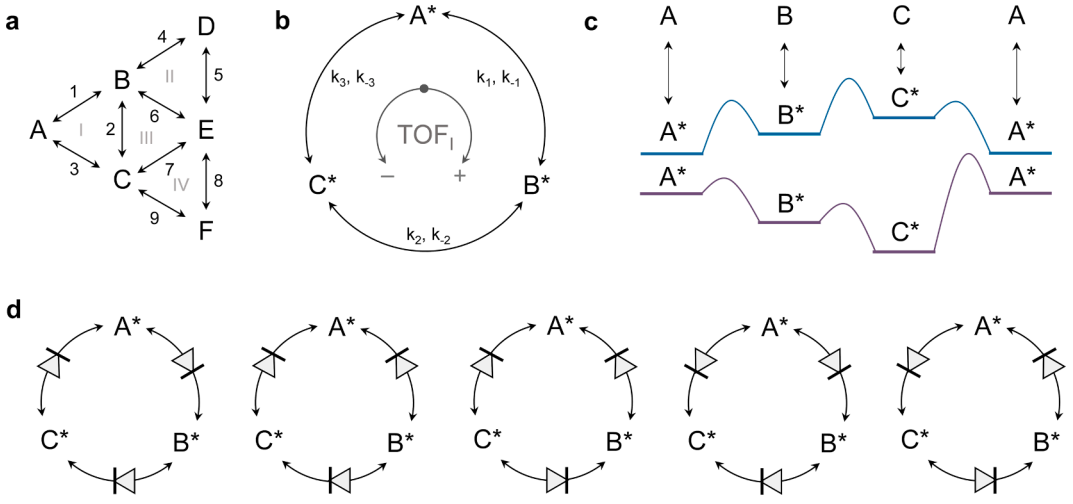

Fig. 1. Catalytic Networks, Loops, and Dynamics. (a) A catalytic reaction network comprised of six surface species and four internal catalytic reaction loops. **(b)** A single catalytic loop of A-to-B-to-C-to-A exhibits positive loop turnover frequency in the clockwise direction and negative loop turnover frequency in the counterclockwise direction. **(c)** The catalytic reaction of A-to-B-to-C-to-A can be programmed to switch between two states with varying intermediate and transition state energies. **(d)** Directionality resulting from kinetic asymmetry drives reactions forward or backward, which in the triangle reaction can exist in multiple permutations of collective molecular flow.

rather than promoting reactions towards the desired overall reaction product. This challenge becomes more complex in more complex reaction networks (Fig. 1**a**) where multiple small catalytic loops can combine to interact or form larger loops comprised of four or more species. A fundamental understanding of the net flux of molecules around a catalytic loop in a programmable catalyst is needed to understand the extent of oscillatory net flow of molecules, the directionality of catalytic loops, and strategies to control them for the benefit of controlling catalytic reaction networks.

In this work, the loop reaction depicted in Fig. 1**b** was simulated to understand the conditions leading to net positive or net negative loop turnover frequencies. Through variation of the dynamic parameters (e.g., frequency) and the chemical reaction scaling parameters defining the catalyst surface, the behavior of the reaction network system and its response to catalytic perturbation was explored to identify classes of unique behavior. Initial simulations demonstrated case studies of chemical and dynamic parameters leading to nonzero loop turnover frequencies, with presentation of dynamic steady state solutions (i.e., limit cycles) highlighting the general behavior of catalytic loops in dynamic operation. This strategy demonstrated the potential for molecules to flow in catalytic loops, to oscillate between only two of three species, or for perturbations to limit reactions to single surface species. Finally, more complicated surface programs were shown to provide capability to control the loop turnover frequency, with variation of the input determining clockwise or counterclockwise molecular flow.

2. Methods

The reaction network was modeled using Julia 1.9.0 and computational resources at the Minnesota Supercomputing Institute (MSI). The model accounts for surface conversion of A*, B*, and C*; adsorption and desorption energies were considered too large to contribute to the chemical system (molecules stayed on the surface), and a thermoneutral reaction, ΔG of the gas phase conversions is zero. The microkinetic model includes for three elementary steps, each a unimolecular, reversible surface reaction,

$$A^* \leftrightarrow_{K_1} B^* \tag{2}$$

$$B^* \leftrightarrow_{K_2} C^* \tag{3}$$

$$C^* \leftrightarrow_{K_3} A^* \tag{4}$$

The binding energy of each species changes in accordance with the forced dynamic nature of the perturbation to the catalyst. The model describes the catalytic state through the descriptor of the binding energy of species A* ($-\Delta H_A = \mathrm{BE_A}$) and the forced perturbation of the catalyst state through the amplitude of the imposed waveform ($\Delta U_A = \Delta BE_A$). This oscillation is defined also by a frequency, f, a waveform shape, and a duty cycle, φ, defined as the fraction of a full oscillation spent in catalyst state 1.

In specifying the reaction coordinate for a given catalytic state, the binding energies of the adsorbed species B* and C*, as well as the activation energy for all three reactions, are defined relative to the binding energy of species A*. The binding energies of the other adsorbed species, B* and C*, are modeled using linear scaling relationships, defined through two parameters: gamma, γ, and delta, δ. γ represents the linear slope between driven changes in the binding energy of species A* to that of species B* and C*, while δ represents the catalytic state in which two surface species have equivalent surface enthalpy [16,23].

$$\gamma_{B-A} = \frac{\Delta BE_B}{\Delta BE_A} \tag{5}$$

$$BE_A = \delta_{B-A};\ BE_B = \delta_{B-A} + \Delta H_{rxn,A\to B} \tag{6}$$

Utilizing these two parameters to define the binding energies of species B* and C* in terms of the binding energy of A* yield equations (6) and (7), as derived the supporting information, under the assumption of a thermoneutral reaction.

$$BE_B = \gamma_{B-A} BE_A + (1-\gamma_{B-A})\delta_{B-A} \tag{7}$$

$$BE_C = \gamma_{C-A} BE_A + (1-\gamma_{C-A})\delta_{C-A} \tag{8}$$

Variation of binding energy was evaluated on the order of ~ 1 eV. Existing experimental methods including temperature programmed desorption and grazing incidence infrared spectroscopy have measured binding energy variation of carbon monoxide by ~ 0.2 eV on HfO_2-based catalytic condenser devices with capacitance of 200-to-300 nF/cm^2 [19,29]. More recently, ion gel catalytic condensers have achieved capacitance as high as 20,000 nF/cm^2 [30], indicating that binding energy can potentially be varied at least an order of magnitude higher than previous measurements.

The activation enthalpies of the forward direction of each unimolecular elementary step are defined using the Brønsted-Evans-Polanyi relationship, which assumes a linear correlation between the activation energy and the heat of surface reaction [31–33]. For the first elementary step of the cyclic reaction, the activation energy can be determined in all catalyst states by equation (9).

$$E_{a,A} = \alpha_1 \Delta H_{R,1} + \beta_1 \tag{9}$$

Definition of the three binding energies and three activation energies at each catalytic state provides the necessary information to form a full microkinetic model of the surface reaction. In computation of the forward rate constants, the pre-exponential factors were calculated using transition state theory, assuming a transmission coefficient of 1, such that the pre-exponential is $\frac{k_B T}{h}$, computed at the set reaction temperature. Equilibrium rate constants arise from the definition of thermodynamic equilibrium, and the reverse rate constant is yielded from the other two to ensure thermodynamic consistency. For this model, the entropy change for the surface reaction is assumed to be negligible relative to the heat of surface reaction.

In accordance with the principle of microscopic reversibility, it also stands that for each catalyst state individually, $k_3 k_2 k_1 = k_{-1} k_{-2} k_{-3}$, which yields the reciprocal relationship in Equation (1).

Rate equations were formulated for each elementary step in accordance with mass-action kinetics. As this model only accounts for the conversion on the surface of the catalyst, with no absorption or desorption of the species, the total surface coverage of species was set to 1.0 such that there are no vacant sites ($\theta^* = 0$). Full derivation of the microkinetic model can be found in the supporting information.

Catalyst oscillation was modeled using a variety of waveforms. In the case of a square waveform, the catalyst is in only one state at a time and switches instantaneously between states; this waveform shape can be applied to a system including two or more distinct catalyst states. When integrating systems with square waveform dynamics, callbacks were implemented to provide continuous integration across the instantaneous changes in catalyst states. Sinusoidal waveforms were also evaluated by including a temporal dependence of the catalyst descriptor such that the integrator varies the binding energy of species A as it solves the species balances. The sinusoidal waveform begins at the lower endpoint of catalyst oscillation, referred to as state 1 in the square waveform case, and exhibits an oscillation amplitude, such that the highest binding energy obtained is consistent with catalyst state 2, in a two state square waveform system. The frequency of oscillation is defined the same in both sinusoidal and square waveforms.

The reaction model was integrated using Rosenbrock23 in Julia 1.9.0. Integration was performed with a relative tolerance of 10^{-8} and an absolute tolerance of 10^{-10}. A maximum number of oscillations was preselected and set sufficiently high to allow for all simulations to converge on their steady state solution. For the simulations in this work, 10,000 s of reaction was sufficient time.

Once the maximum number of oscillations was set, the callback set responsible for periodic changes to the catalyst surface was defined. The callback set was expanded to include a periodic check for steady state after every ten oscillations. The condition for steady state was defined using the time-average of each elementary rate over two oscillations. Once the difference between those time-averaged quantities was less than a set tolerance of 10^{-5}, the integration was terminated. This difference was computed as a percent difference for time-averaged rates greater than one and an absolute difference for time-averaged rates less than one. This analysis effectively checked that each elementary rate was equal within the set tolerance ($\bar{r}_1 = \bar{r}_2 = \bar{r}_3$). Upon terminating the integration, the solution was returned. At dynamic steady-state (i.e., limit cycle), no species accumulate on the surface, motivating the analysis of the time-averaged elementary rates over complete catalytic oscillations previously outlined.

Ternary plots provided graphical representation of the surface coverages of all three species with the progression of time. Python 3 and the python-ternary matplotlib plotting library were used to create ternary plots from imported data compiling the surface coverages of each surface species in time.

The loop reaction was specified through eleven chemistry parameters (three sets of α and β, two sets of γ and δ, and $\theta_{species}$), five dynamic parameters (oscillation start point BE_A, amplitude ΔBE_A, frequency f, surface waveform shape, and the duty cycle of the waveform), and the reaction temperature (T) defined in Table 1. As this model addressed only a surface reaction, the initial surface coverages of each species was set prior to integration, most often being equal coverages of each species ($\theta_A = \theta_B = \theta_C = 1/3$ at t = 0), except in the cases for exploring the effect of varying the initial coverages.

3. Results and discussion

Evaluation of the triangle reaction under dynamic conditions is complicated by the large parameter space needed to fully specify three elementary reactions and the variation of catalytic states. For this reason, simulations considered several case studies of parameter sets that exhibit unique behavior including positive or negative loop turnover frequency, oscillation between two conditions, termination at a single concentration, or three state programs that drive reactions either forward or backward.

The loop turnover frequency is defined as the time-averaged elementary rate of net reaction about the loop over one period of oscillation. Once the oscillation had progressed to a limit cycle (i.e., dynamic steady state), each time-averaged rate of reaction within the loop was equivalent, allowing any one of the three elementary rates to be integrated. Using mass action kinetics, the data returned from the simulation for the surface coverage of each species as a function of time was converted into three arrays to quantify the elementary rates as a function of time. The time-averaged rate was determined by integrating forward and reverse elementary rates from the start of a cycle (t_1) to the end of a cycle (t_2) and then dividing by the period,

$$TOF_{LOOP} = \frac{\int_{t_1}^{t_2}(r_1(t) - r_{-1}(t))dt}{t_2 - t_1} = \frac{\int_{t_1}^{t_2}(r_i(t) - r_{-i}(t))dt}{t_2 - t_1} \quad (10)$$

where i refers to any of the reactions in the loop ($i = 1$, 2, or 3). The simulation reaction data were integrated using trapezoidal integration between each individual data point, with the limit cycle identified when the loop turnover frequency based on each of the three reaction rates in the loop agreed within 10^{-5} s^{-1}.

3.1. Positive loop turnover frequency

The chemistry parameters of the triangle reaction system were initially selected to evaluate a single case from the substantial full parameter space; the reaction coordinate for the considered loop reaction of A* to B* to C* to A* is depicted in Fig. 2**a**. Upon programmed changes in the binding energy of A*, driven by catalyst perturbation between state 1 and 2, the binding energies of species B* and C* as well as the activation energy of each elementary step shifted accordingly. For this set of selected parameters, both gamma relationships, $\gamma_{B-A} = 1.5$ and $\gamma_{C-A} = 0.5$, were positive indicating that the binding energies all changed in the same direction (i.e., strengthened when moving from state 1 to state 2).

Application of a square wave to the catalyst yielded a periodic solution of surface coverages and elementary rates versus time, as shown in Fig. 2**b**. When starting initially in state 1 with equal coverages of A*,

Table 1
Model parameters for forced dynamic simulations.

Parameter	Units	Description
α_1	None	Bronsted-Evan-Polanyi (BEP) relationship slope, the proportionality constant between the heat of the surface reaction A ← → B and the activation energy of the forward direction of the reaction.
α_2	None	BEP proportionality constant for B ← → C.
α_3	None	BEP proportionality constant for C ← → A.
β_1	eV	BEP relationship constant offset. A constant defining the activation energy of the forward direction of A ← → B in the case of the elementary step being energetically neutral (heat of the surface reaction equals zero)
β_2	eV	BEP constant offset for B ← → C.
β_3	eV	BEP constant offset for C ← → A.
γ_{A-B}	None	Linear scaling relationships, the proportionality constant defining the linear slope between driven changes in the binding energy of species A to the corresponding change in binding energy of species B.
γ_{A-C}	None	Linear scaling relationships, the linear slope between driven changes in the binding energy of species A to the corresponding change in binding energy of species C.
δ_{A-B}	eV	Linear scaling relationships, a constant representing the catalytic state in which surface species A* and B* have equivalent surface enthalpies. δ_{A-B} is equal to the surface enthalpy at which this occurs.
δ_{A-C}	eV	Linear scaling relationships, a constant representing the catalytic state in which surface species A* and C* have equivalent surface enthalpies. δ_{A-C} is equal to the surface enthalpy at which this occurs.
$\theta_{species}$	None	The total surface coverage of all bound species. In the absence of absorption and desorption, the number of empty catalytic sites is constant. The total surface coverage is equivalent to 1 minus the surface coverage of the vacant sites.
Temperature (T)	K	The temperature of the reactor, dictating the temperature at which the reaction proceeds.
BE_A	eV	Lower bound of catalytic perturbation. Starting state of the catalyst as described by the binding energy of species A, which is equivalent to the additive inverse of the heat of adsorption of species A.
ΔBE_A	eV	The amplitude of the dynamic oscillation. In the case of a square waveform this marks the difference between the binding energy of A in state 1 vs. state 2. In a sinusoidal case, this marks half the distance between the upper and lower bounds of perturbation.
f	s^{-1}	The frequency of oscillation, the inverse of the time it takes for one whole oscillation of the catalyst.
Surface waveform shape		Describes the shape of the waveform of catalytic perturbation. In a square waveform, the catalyst switches in between two states instantaneously. In a sinusoidal waveform the catalyst oscillates between an upper and lower bound, such that the binding energy of species A has a sinusoidal dependence on time.
Duty Cycle	%	For square waveforms, the duty cycle describes the fraction of one oscillation spent in catalyst state 1. One minus the duty cycle describes the fraction of one oscillation spent in catalyst state 2.

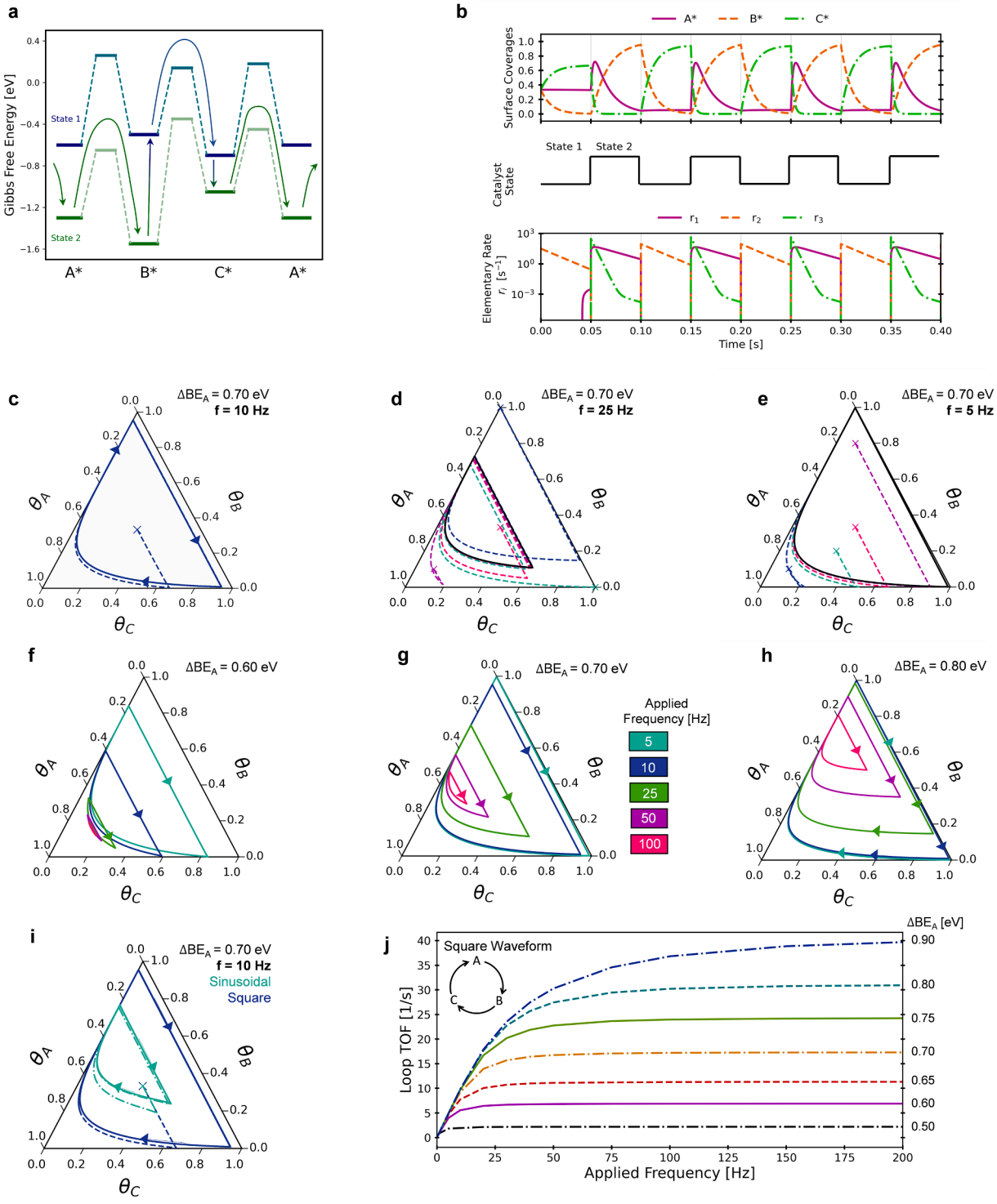

Fig. 2. Positive loop turnover frequency in the triangle surface reaction. Simulated data in each panel uses the same chemical dynamic parameters ($\alpha_A = 0.6$, $\alpha_B = 0.8$, $\alpha_C = 0.8$, $\beta_A = 0.8$ eV, $\beta_B = 0.8$ eV, $\beta_C = 0.8$ eV, $\gamma_{B-A} = 1.5$, $\gamma_{C-A} = 0.5$, $\delta_{B-A} = 0.8$ eV, $\delta_{C-A} = 0.8$ eV). The reaction temperature (T = 298.15 K) and the minimum binding energy of A* corresponds to state 1 ($BE_{A,1} = 0.6$ eV) for all simulations. **(a)** State-energy diagram of the programmable catalyst switching between state 1 and state 2, with an amplitude of oscillation of $\Delta BE_A = 0.7$ eV. **(b)** Square wave perturbation of the catalyst yields a periodic variation for the surface coverage of each species and each elementary rate. The elementary rates are predominantly positive, with only rate 2 switching to slightly negative in catalyst state 2, indicating a positive loop turnover frequency. The initial condition for this simulation involved equal coverages of A*, B*, and C*; such that initially: $\theta_A = \theta_B = \theta_C = 1/3$. **(c)** Ternary plot of the surface coverages from panel b. **(d-e)** Variation of the initial surface coverages of A*, B*, and C*, indicating the start of the simulation with an x. All initial surface coverages lead to dynamic convergence of the same limit cycle. **(f-h)** Effect of amplitude and frequency of oscillation on the limit cycle of surface coverages. **(i)** Effect of waveform shape on the limit cycle of surface coverages. **(j)** Dependence of the loop turnover frequency of the reaction on the dynamic parameters dictating catalyst perturbation: applied frequency and amplitude of oscillation.

B*, and C* ($\theta_A = \theta_B = \theta_C = 1/3$), all B* molecules on the surface reacted to form C*. In state 1, C* is in an energetic low state, leading to its accumulation on the surface. Then, when the catalyst switched to state 2, C* weakened in binding energy relative to A*, such that the forward reaction was favorable leading to the generation of A* on the surface, then B*. As the oscillation continued, switching between the two catalyst states promoted the formation of a full loop reaction, with no net accumulation of a given species on the surface. After the first check for steady state, this system reached the steady state limit cycle, yielding a loop turnover frequency of 9.18 s^{-1}. In other words, 9.18 mol of molecules per mole of catalytic sites per second traverse the catalytic loop (A* to B* to C* to A*) when a square wave was applied to the catalyst surface at 10 Hz.

The evolution of the catalytic surface depicted in Fig. 2**b** was also represented with a ternary plot in Fig. 2**c** of the three surface species, A*, B*, and C*, which at all times summed to unity when there were no open sites ($\theta^* = 0$). Starting from the middle of the ternary diagram, the initial reaction trajectory (dashed line) moved outward first increasing in C*. Upon the switch in catalyst state, A* began to accumulate which reacted to form B*, as evident by the curved portion of the limit cycle. After two complete oscillations, the trajectory reached the steady state solution limit cycle identified as the thick continuous line. Every subsequent square wave cycle moved along the limit cycle, which for this set of chemical and dynamic parameters was close to the ternary plot boundaries associated with high coverages of B* and C*.

An important behavior of the oscillating triangle reaction was the convergence of the reaction to a limit cycle independent of initial conditions. As shown in both Fig. 2**d and 2e**, variation of the initial surface coverages for the selected set of dynamic parameters yielded dynamic convergence upon the same limit cycle, providing evidence that within the spatial limits of the defined problem, there existed only one dynamic steady-state solution. Reactions with initial surface coverages inside the final limit cycle exhibited trajectories that moved outward in the ternary plot, while reactions with initial surface coverages outside the final limit cycle displayed trajectories that moved inward, toward the limit cycle.

The speed of convergence of the reaction trajectory to a limit cycle at oscillatory steady state depended on the amplitude and frequency of the catalyst oscillation. Increasing the frequency of oscillation from 10 Hz in Fig. 2**c to 25** Hz in Fig. 2**d** decreased the time the catalyst stays in each state and yielded a smaller overall limit cycle within the ternary diagram. Alternatively, decreasing the frequency of catalyst oscillation to 5 Hz in Fig. 2**e** increased the time the catalyst remained in each state and produced a large overall limit cycle within the ternary diagram. This behavior was consistent with the energy diagram of Fig. 2**a**; in either state, one surface species was lowest in energy such that fixed catalyst conditions eventually yielded a θ_C of $\sim$ 1.0 in state 1 and a θ_B of $\sim$ 1.0 in state 2. Therefore, at low frequencies, sufficient time was provided for the reaction to achieve static equilibrium in each catalyst state, and the trajectory was observed to approach the respective corner of the ternary plot. Alternatively, a rapidly switching catalyst did not provide sufficient time for the reaction to progress far from the middle of the ternary plot yielding small overall limit cycles.

Variation of the catalyst waveform shape varied the productivity of the reactive loop. Because a square waveform shape spent a greater amount of time at the two extreme boundaries of the catalyst oscillation, it exhibited a greater conversion of molecules on the surface relative to a sinusoidal wave form, as shown in Fig. 2**i.** Application of a square waveform oscillation produced a loop turnover frequency of 9.18 s^{-1}, while the sinusoidal oscillation produced a loop turnover frequency of only 4.97 s^{-1}.

Analysis of a loop turnover frequency provided insight into both the directionality of the loop and the rate at which molecules circulated on the surface. An increase in the applied frequency of oscillation yielded a higher loop turnover frequency. Despite lower conversion on the surface at high frequencies, as depicted by the smaller steady-state limit cycles in Fig. 2**f-2 h, a** higher frequency yielded an increased rate at which the molecules move around the loop. With the increase of the applied oscillation frequency at a given amplitude of oscillation, the loop turnover frequency exhibited asymptotic behavior as it increased before reaching its maximum potential loop turnover frequency, as shown in Fig. 2**j**. At low applied frequencies (<0.1 Hz), a small, almost negligible, loop turnover frequency was observed. With increasing amplitude of oscillation, the 'molecular pumping' effect of the dynamic catalyst became more powerful, yielding higher loop turnover frequency at a given applied frequency.

3.2. Negative Loop turnover frequency

The chemistry parameters of the triangle reaction system were changed to evaluate a new case in which the molecules reacted in a counterclockwise direction, corresponding to a negative loop turnover frequency, as opposed to the clockwise direction in the previous case, which corresponded to a positive (by definition) loop turnover frequency. The reaction coordinate energy diagram for the considered loop reaction of A* to C* to B* to A* is depicted in Fig. 3**a**.

For the dynamic catalyst operating at 10 Hz, a periodic solution resulted for the surface coverages and elementary rates versus time, as shown in Fig. 3**b**. Starting with equal surface coverages of all surface species with the catalyst in state 1, all C* on the surface reacted to form B*. Upon switching to catalyst state 2, the B* reacted to form A*, which proceeded to form C*. As oscillation continued, a full loop formed such that the reaction proceeded from A* to C* to B* to A*, a counterclockwise route about the loop reaction. The elementary rates of this reaction were less than 0, confirming the flow of molecules in the negative direction. The system rapidly approached a steady-state limit cycle, depicted in Fig. 3**c**, achieving a loop turnover frequency of -8.76 s^{-1}.

The loop turnover frequency for this reaction was negative for all variations of the evaluated oscillation frequency and amplitude. As shown in Fig. 3**d**, increasing the applied frequency resulted in a more negative loop turnover frequency. Despite the lower conversion of molecules in one oscillation, as seen by the limit cycles that shrink with increasing frequency in Fig. 3**e-3 g**, the increase in number of oscillations per second drove an increase in molecular flux on the surface in the counterclockwise direction, consistent with a more negative loop turnover frequency. Increasing the amplitude of oscillation led to a more negative loop turnover frequency and higher conversion on the catalyst surface. Increasing the amplitude of oscillation enhanced the 'catalytic molecular pumping' effect of the dynamic surface. Increased amplitude lead to a greater input of energy to drive the reaction in a loop, as revealed through the increase in the absolute value of the loop turnover frequency, consistent with the same observation in the positive loop turnover frequency case.

3.3. Catalyst Surface Poisoning

Application of dynamic catalyst surfaces to the triangle reaction resulting in a net flow of the molecules in a loop does not necessarily extend to all parameter sets. One case in which dynamic oscillation produces a negligible loop turnover frequency involves a steady-state solution in which one catalyst species covers all available catalyst sites. This behavior, sometimes referred to as 'poisoning' of the catalyst surface, occurs when one species binds to the catalyst surface at a higher binding energy than all other species. In the case of a dynamic catalyst, if one species binds most tightly to the surface such that it is thermodynamically favored in all catalyst states, that species will accumulate on the surface as oscillation proceeds with time until all catalyst sites are occupied by that species.

This behavior was simulated for the triangle reaction for three distinct cases under dynamic operation (*f* of 10 Hz): (i) high coverage of A*, (ii) high coverage of B*, and (iii) high coverage of C*. As shown in Fig. 4**a**, a triangle reaction with A* most tightly bound to the surface at both catalyst states was simulated. Application of catalyst oscillation

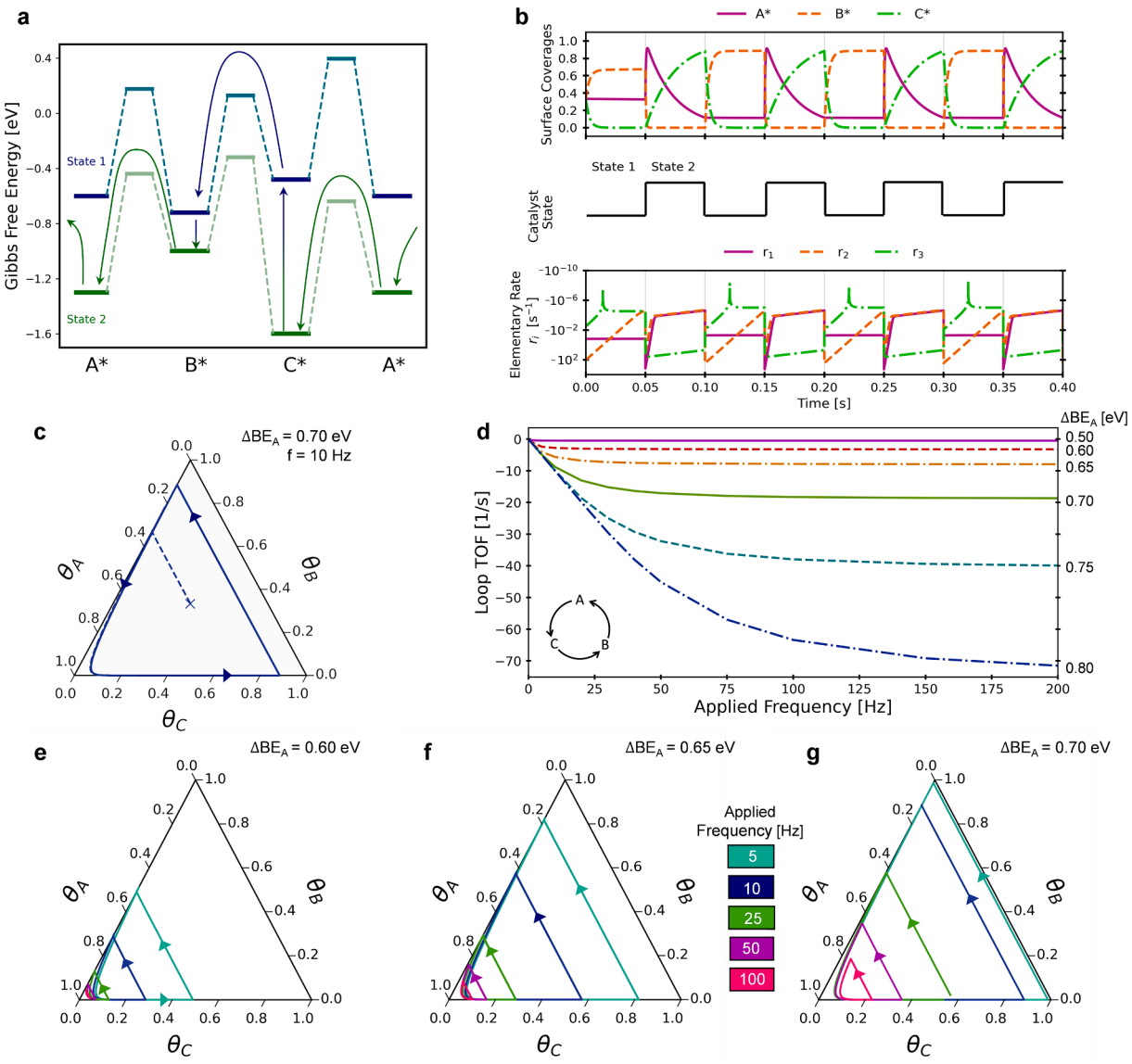

Fig. 3. Negative loop turnover frequency in the triangle surface reaction. Simulated data in each panel uses the same chemical dynamic parameters ($\alpha_A = 0.2$, $\alpha_B = 0.2$, $\alpha_C = 0.2$, $\beta_A = 0.8$ eV, $\beta_B = 0.8$ eV, $\beta_C = 0.9$ eV, $\gamma_{B-A} = 0.4$, $\gamma_{C-A} = 1.6$, $\delta_{B-A} = 0.8$ eV, $\delta_{C-A} = 0.8$ eV,). The reaction temperature (T = 298.15 K) and the minimum binding energy of A* corresponds to state 1 ($BE_{A,1} = 0.6$ eV) for all simulations. **(a)** State-energy diagram of the programmable catalyst switching between state 1 and state 2, with an amplitude of oscillation of $\Delta BE_A = 0.7$ eV. **(b)** Square wave perturbation of the catalyst yields a periodic variation for the surface coverage of each species and each elementary rate. The elementary rates are always positive indicating a positive loop turnover frequency. The initial condition for this simulation involved equal coverages of A*, B*, and C*; such that initially: $\theta_A = \theta_B = \theta_C = 1/3$. **(c)** Ternary plot of the surface coverages from panel b. **(d)** Dependence of the loop turnover frequency of the reaction on the dynamic parameters dictating catalyst perturbation: applied frequency and amplitude of oscillation. **(e-g)** Effect of amplitude and frequency of oscillation on the limit cycle of surface coverages.

with initially equal coverage of each species on the surface ($\theta_A = \theta_B = \theta_C = 1/3$) lead to the depletion of B* and C* and generation of A* with time as the system approached steady state. The steady-state solution was $\theta_A = 1.0$, with negligible amounts of B* and C* on the surface. Plotting the simulated data on a ternary plot, shown in Fig. 4**b**, displays a trajectory that moves from the initial conditions at the center of the plot, denoting equal surface coverage of all three species, to the bottom left corner of the plot, denoting complete coverage of A*.

Achieving complete coverage of B* on the surface was depicted in Fig. 4**c-4d**, as a reaction energy diagram for B* to be most tightly bound in both catalyst states. As oscillation proceeded, C* and A* depleted, producing a surface coverage trajectory that moved from the center of the plot to the top corner, denoting a steady state solution of $\theta_B = 1.0$.

Similarly, achieving complete coverage of C* on the surface is depicted in Fig. 4**e-f**. This dynamic reaction energy diagram was generated by changing the values of γ_{B-A} and γ_{C-A} from the previous case, now resulting in C* as the most tightly bound surface species. The activation barriers were also modified to yield favorable reaction to C* from the other surface species. Oscillating the catalyst surface promoted the depletion of B* and A*. In Fig. 4**f**, it was apparent by the two straight portions of the trajectory that B* reacted to C* more readily than A*, which was simply a consequence of the energy barriers as defined by the selected reaction parameters. The reaction trajectory began at the center of the plot and moved towards the bottom right corner, denoting complete coverage of C* and a steady state solution of $\theta_C = 1.0$.

Each of these three cases correspond with a steady state solution of one species covering all available catalyst sites; however, this lack of observable molecular flow about the loop does not imply a loop turnover frequency of zero. Rather, in each of the three cases, there is a small, but non– zero loop turnover frequency. For an applied frequency of 10 Hz, at

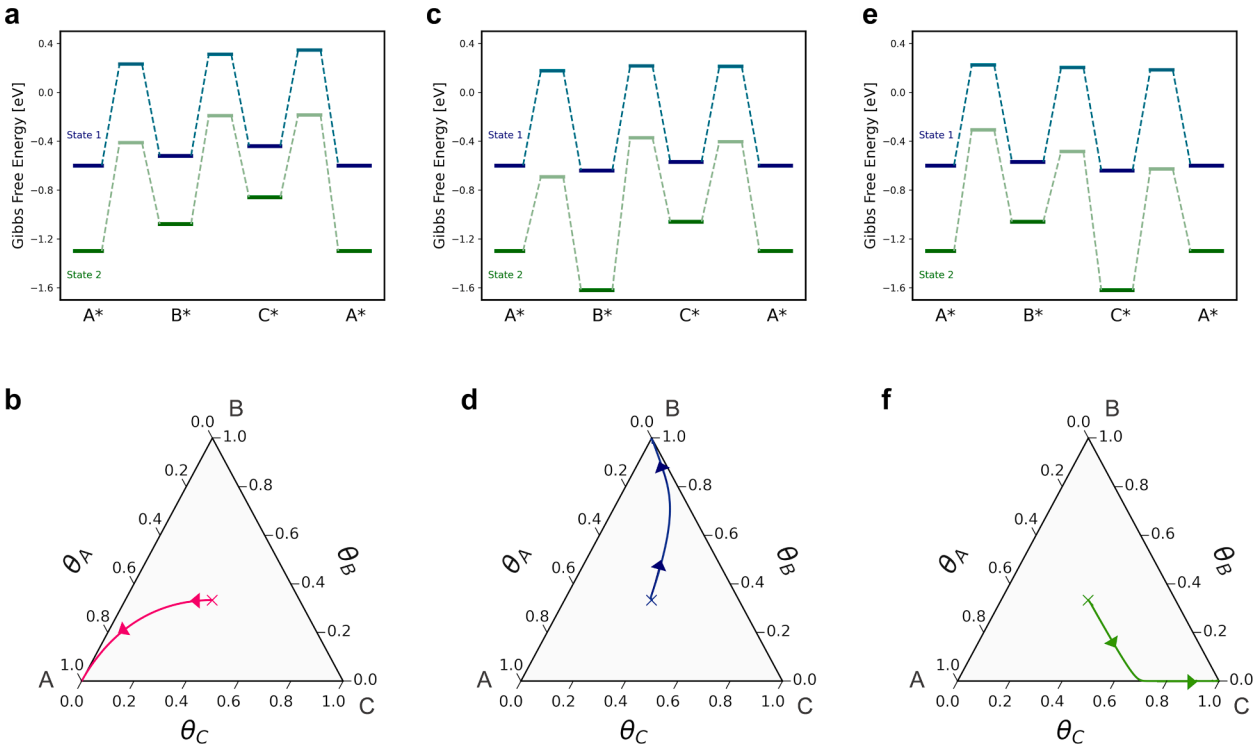

Fig. 4. Favoring of one species on the surface in the triangle surface reaction. Simulated data in each panel uses the same parameters describing the dynamic catalyst surface with an applied square waveform ($BE_A = 0.6$ eV, $\Delta BE_A = 0.7$ eV, f = 10 Hz, ∅= 50 %). **(a)** State-energy diagram of the programmable catalyst switching between state 1 and 2, with the following chemistry parameters: $\alpha_A = 0.4$, $\alpha_B = 0.4$, $\alpha_C = 0.4$, $\beta_A = 0.8$ eV, $\beta_B = 0.8$ eV, $\beta_C = 0.85$ eV, $\gamma_{B-A} = 0.8$, $\gamma_{C-A} = 0.6$, $\delta_{B-A} = 0.2$eV, $\delta_{C-A} = 0.2$eV. **(b)** Ternary plot of the periodic solution from the simulation which leads to full coverage of A* on the surface at steady-state. **(c)** State-energy diagram of the programmable catalyst switching between state 1 and 2, with the following chemistry parameters: $\alpha_A = 0.6$, $\alpha_B = 0.8$, $\alpha_C = 0.6$, $\beta_A = 0.8$ eV, $\beta_B = 0.8$ eV, $\beta_C = 0.8$ eV, $\gamma_{B-A} = 1.4$, $\gamma_{C-A} = 0.7$, $\delta_{B-A} = 0.5$eV, $\delta_{C-A} = 0.5$eV. **(d)** Ternary plot of the periodic solution from the simulation which leads to full coverage of B* on the surface at steady-state. **(e)** State-energy diagram of the programmable catalyst switching between state 1 and 2, with the following chemistry parameters: $\alpha_A = 0.8$, $\alpha_B = 0.4$, $\alpha_C = 0.6$, $\beta_A = 0.8$ eV, $\beta_B = 0.8$ eV, $\beta_C = 0.8$ eV, $\gamma_{B-A} = 0.7$, $\gamma_{C-A} = 1.4$, $\delta_{B-A} = 0.5$eV, $\delta_{C-A} = 0.5$eV. **(f)** Ternary plot of the periodic solution from the simulation which leads to full coverage of C* on the surface at steady-state.

a steady state coverage of $\theta_A = 1.0$, there was a loop turnover frequency of -0.00015 s^{-1}, indicating that in the presence of catalyst perturbation, despite A* being energetically favored, a slight negative loop turnover frequency was still observed. This is similarly observed for the case of $\theta_B = 1.0$ at steady state where the observed loop turnover frequency was 0.0081 s^{-1} and for $\theta_C = 1.0$ which had an observed loop turnover frequency of $-1.3 \bullet 10^{-5}$ s^{-1}. These tiny loop turnover frequencies indicate that even parameter sets that heavily favor surface coverages of a single species exhibit non-zero loop turnover frequencies, even if they might have negligible impact on the overall catalytic reaction rate of a chemical network.

3.4. Oscillation between Two Surface Species

A set of parameters was selected for a reaction that produced a steady state oscillation predominately between two surface species upon oscillatory catalyst perturbation. The reaction coordinate for driven oscillation between B* and C* is depicted in Fig. 5**a**. In both catalyst states 1 and 2, A* remained highest in energy; therefore, conversion to A* on the surface was never thermodynamically favorable (Fig. 5**b**). In state 1, B* was in an energetically low state, but upon a switch to state 2, C* became most tightly bound, in an energetically low state. As the switch in the species that is most tightly bound correlated with a switch in the catalyst state, it was intuitive that oscillation between those two species existed as the catalyst oscillated between the two states.

The periodic solution of this dynamic system is depicted in Fig. 5**b** and shown on a ternary plot in Fig. 5**c**. Starting initially with equal surface coverages of each species ($\theta_A = \theta_B = \theta_C = 1/3$), A* depleted on the surface as the catalyst oscillated between states 1 and 2; state 1 promoted the accumulation of B*, and state 2 promoted the accumulation of C*. After three complete oscillations, the system reached steady state oscillation between $\theta_B \sim 1.0$ and $\theta_C \sim 1.0$, as shown by the solid pink line along the right side of the ternary plot in Fig. 5**c**.

Increasing the frequency of oscillation decreased the time the catalyst existed in each catalyst state, thereby limiting the conversion of B* to C* in state 2 and C* to B* in state 1. Frequencies of 50 Hz and 100 Hz are shown in Fig. 5**d and 5e**. At a frequency of 50 Hz the steady state solution oscillated between $\theta_B = 0.65$, $\theta_C = 0.35$ and $\theta_B = 0.1$, $\theta_C = 0.9$. At a frequency of 100 Hz the steady state solution oscillated between $\theta_B = 0.5$, $\theta_C = 0.5$ and $\theta_B = 0.18$, $\theta_C = 0.82$.

Decreasing the amplitude of catalyst oscillation decreased the extent of surface coverage oscillation between catalyst states. Relative to an amplitude of $\Delta BE_A = 0.7$ eV, decreasing the amplitude to 0.6 eV at both 10 and 100 Hz showed a decrease in the range of oscillating surface coverages (Fig. 5**f and 5 h**), indicative of the decrease in energy provided by catalyst oscillation. In this system, increase of the oscillation amplitude yielded a shift in the range of oscillating surface coverages, producing full surface coverage of C* when the catalyst existed in State 2, as shown in Fig. 5**g**.

3.5. Application of Three Catalyst States

Increasing the complexity of the applied waveform from oscillation between two states to oscillation between three states provided for greater control of the surface reaction behavior. The three catalyst states were defined using the same metrics as a two-state system, where now ΔBE_A indicates the amplitude of oscillation between state 1 and state 3 with state 2 existing equally between them. Chemistry parameters were

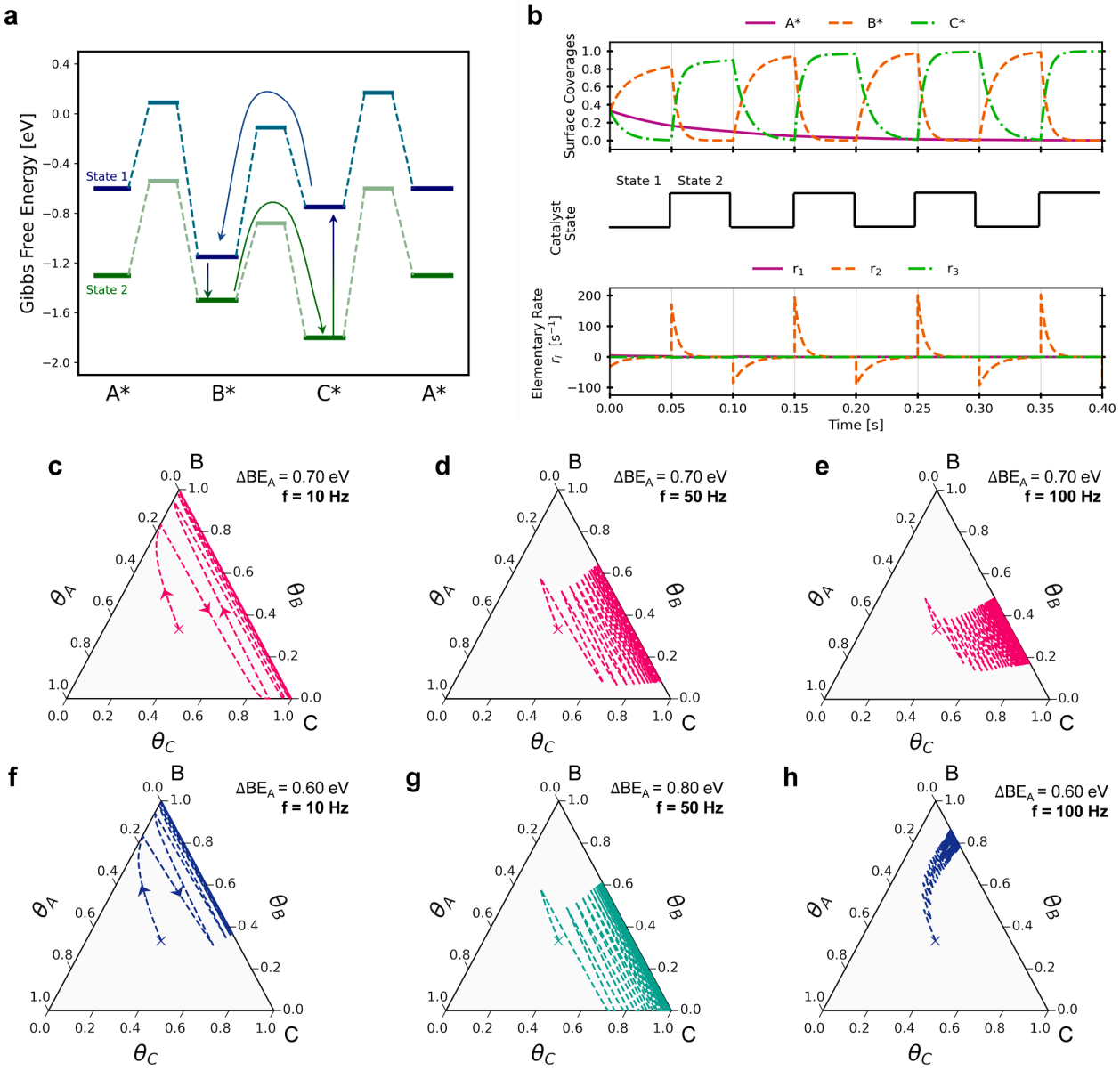

Fig. 5. Oscillation between two surface species. Simulated data in each panel uses the same chemical dynamic parameters ($\alpha_A = 0.2$, $\alpha_B = 0.6$, $\alpha_C = 0.8$, $\beta_A = 0.8$ eV, $\beta_B = 0.8$ eV, $\beta_C = 0.8$ eV, $\gamma_{B-A} = 0.5$, $\gamma_{C-A} = 1.5$, $\delta_{B-A} = 1.7$eV, $\delta_{C-A} = 0.3$ eV,). The reaction temperature (T = 298.15 K) and the minimum binding energy of A* corresponds to state 1 ($BE_{A,1} = 0.6$ eV) for all simulations. **(a)** State-energy diagram of the programmable catalyst switching between state 1 and 2 to drive reaction back and forth between B* and C*. **(b)** Square wave perturbation of the catalyst applied at a frequency of 10 Hz yields depletion of A* on the surface and reaction back and forth between B* and C*. **(c)** Ternary plot depicting the data shown in b. **(d-e)** Increasing the applied frequency of catalyst oscillation. **(f-h)** Decreasing the amplitude of oscillation decreases the energy provided to drive molecular oscillation, while increasing the amplitude results in a shift in the range of oscillation.

selected such that each catalyst state corresponded with the formation of one of the surface species (i.e., that species was lowest in energy). As illustrated in Fig. 6**a,** state 1 favored full coverage of C* at equilibrium, state 2 yielded A*, and state 3 yielded B*. Since each state favors its own species, it was proposed that the order of catalyst states in which the oscillation is applied can control the direction of molecular flow about the loop.

Application of a waveform that switched the catalyst surface from state 1 to 2 to 3 and then back to state 1 yielded the periodic solution of surface coverages and elementary rates shown in Fig. 6**b**. Starting with equal coverages of each species ($\theta_A = \theta_B = \theta_C = 1/3$) in state 1, all A* and B* reacted on the surface to form C*. Upon switching to catalyst state 2, A* increased in binding energy relative to C*, allowing for the promotion of the forward reaction of C* to A*. Upon switching to state 3, B* increased in binding energy relative to A*, promoting the reaction of A* to B*. Returning to state 1, C* increased in binding energy relative to B*, promoting the forward reaction and returning to a surface covered in C*.

As oscillation continued, the system approached a dynamic steady-state in which there was a net clockwise flow of molecules on the surface, illustrated in Fig. 6**c**, yielding a positive loop turnover frequency of 2.41 s^{-1}. Fig. 6**c** also highlights a reversal of the loop turnover frequency at high coverages of C*, which corresponded to the switch from state 1 to 2. When the catalyst existed in state 2 with a high coverage of C*, C* reacted preferentially forward to form A*, yet a leak in the molecular rachet allowed for a small portion of C* to react in the reverse direction to form B*. B* continued reacting to A*, which produced the counter-clockwise loop in the lower left corner of the ternary plot. Similar to a two-state oscillation system, increasing the frequency of oscillation of the waveform decreased the size of the surface coverage limit cycle, shown in Fig. 6**d**, which reflected a decrease in the number of molecules

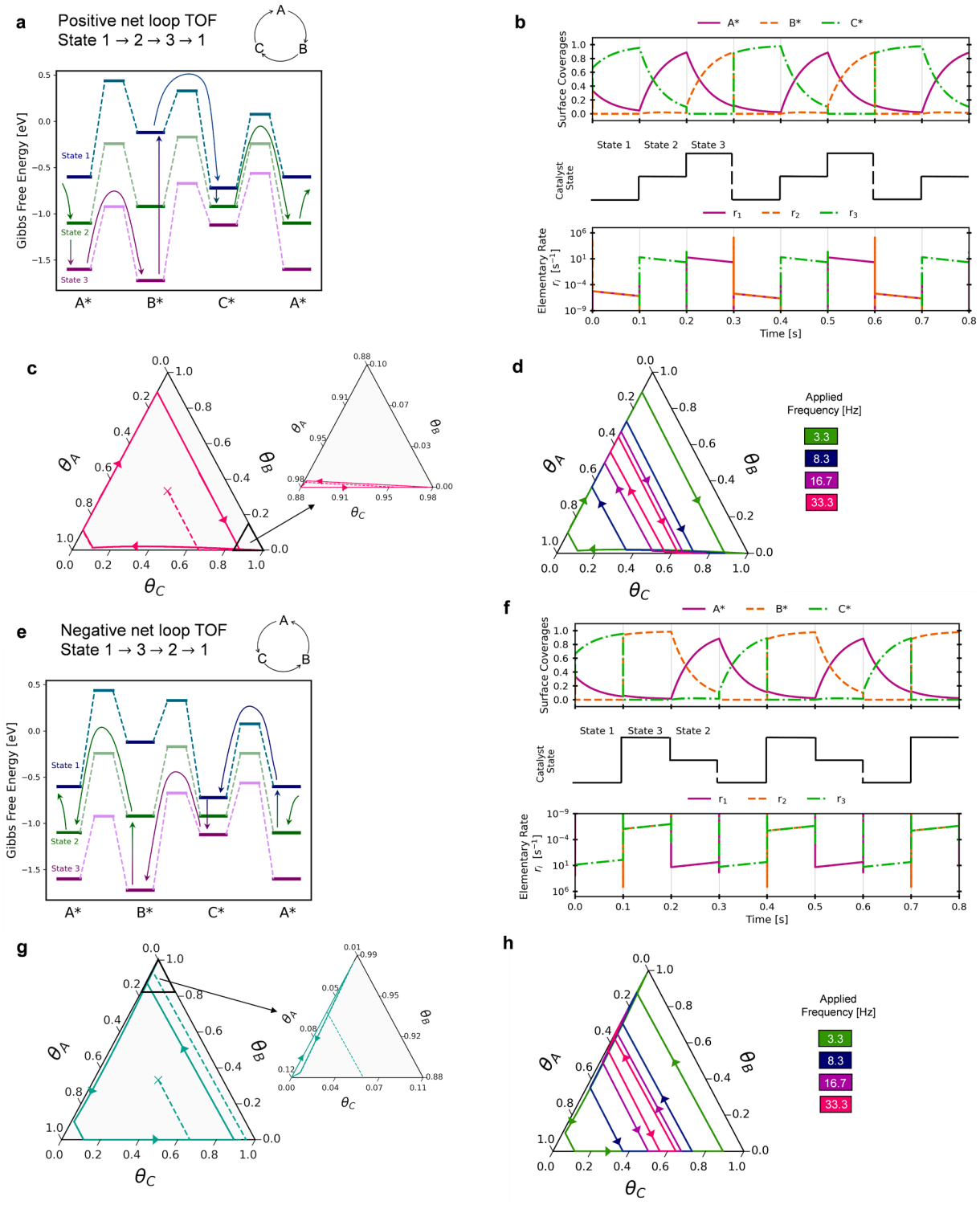

Fig. 6. Oscillation between three catalyst states. The data simulated in each panel is described by the same chemistry parameters: $\alpha_A = 0.6$, $\alpha_B = 0.5$, $\alpha_C = 0.4$, $\beta_A = 0.75$ eV, $\beta_B = 0.75$ eV, $\beta_C = 0.75$ eV, $\gamma_{B-A} = 1.6$, $\gamma_{C-A} = 0.4$, $\delta_{B-A} = 1.4$eV, $\delta_{C-A} = 0.8$eV. **(a)** State-energy diagram of three distinct catalytic states. The minimum binding energy is associated with state 1, defined by $BE_A = 0.6$ eV. The total amplitude of oscillation between state 1 and 3 is $\Delta\ BE_A = 1.0$ eV, with an amplitude of $\Delta\ BE_A = 0.5$ eV between states 1 and 2. A positive loop turnover frequency is induced by switching from state 1 to 2 to 3 then back to 1. **(b)** Application of a square waveform to the catalyst at a frequency of 3.3 Hz, with a duty cycle of 33.3 % (spending equivalent time in each of the three states), oscillating in the order of state 1 to state 2 to state 3, then back to state 1, yields a net turnover frequency of 2.4 s^{-1}. **(c)** Ternary plot of the data in (b) indicating clockwise circumfluence about the loop reaction. Zooming in on the bottom left corner of the plot reveals a portion of the loop exhibiting molecular flow in the negative direction. **(d)** Effect of applied frequency on the limit cycle of the 3 state system. **(e)** State-energy diagram of the same three catalyst states. A negative loop turnover frequency is induced by switching from state 1 to 3 to 2 then back to 1. **(f)** Application of a square waveform to the catalyst at a frequency of 3.3 Hz, with a duty cycle of 33.3 % (spending equivalent time in each of the three states), oscillating in the order of state 1 to state 2 to state 3, then back to state 1, yields a net turnover frequency of −2.4 s^{-1}. **(g)** Ternary plot of the data in (f) indicating counterclockwise circumfluence about the loop. A small loop of the opposite direction forms in the top corner of the plot. **(h)** Effect of applied frequency on the limit cycle of the 3 state system.

reacting on the surface per oscillation.

Application of the three-state square waveform in the reverse order effectively reversed the circumfluence of species on the surface. Switching from state 1 to 3 to 2 and then back to 1, as outlined in Fig. 6**e**, yielded a periodic solution, generating species in the order C*→ B*→ A*→ C*. Fig. 6**f** illustrates the periodic solution and the formation of species in each catalyst state, starting from equal coverages of each species ($\theta_A = \theta_B = \theta_C = 1/3$).

After the first check of steady state, this system had reached a dynamic steady state in which there was a net counterclockwise flow of molecules, shown in Fig. 6**g**, producing a negative loop turnover frequency of -2.41 s^{-1}. In this oscillation order, state 2 still exhibited a leak in the molecular rachet through a brief reversal of the loop turnover frequency. As the catalyst switched from state 3 to 2, there was a high coverage of B* and although B* preferentially reacted in the reverse direction to A*, a small portion of B* leaked forward, reacting to form C*. This behavior is illustrated by the small clockwise loop in the inset of Fig. 6**g**. This system was consistent with the positive system as increasing the frequency of oscillation decreased the number of molecules that reacted in one catalyst oscillation, as apparent through the decreasing sizes of limit cycles in Fig. 6**h**.

Simplifying this three-state system back into two states (by eliminating one of the three states) altered the behavior of the reactive loop and significantly reduced the extent of loop turnover frequency; however, this alternative case provides understanding of the three-state system. Isolating state 1 and 2 (and eliminating state 3), illustrated in the state-energy diagram in Fig. 7**a**, promoted oscillation between A* and C* on the catalyst surface. Switching from catalyst state 1 to 2 promoted the reaction of C* to A*, while switching from state 2 to 1 promoted the reverse reaction of A* to C*. The use of catalyst state 2 allowed for the leakage of C* to B* when there was high coverage of B* at the onset of switching to state 2. This slight leak in the molecular ratchet yielded a small negative loop turnover frequency of -0.14 s^{-1}, depicted by the counterclockwise direction of the limit cycle in Fig. 7**b**.

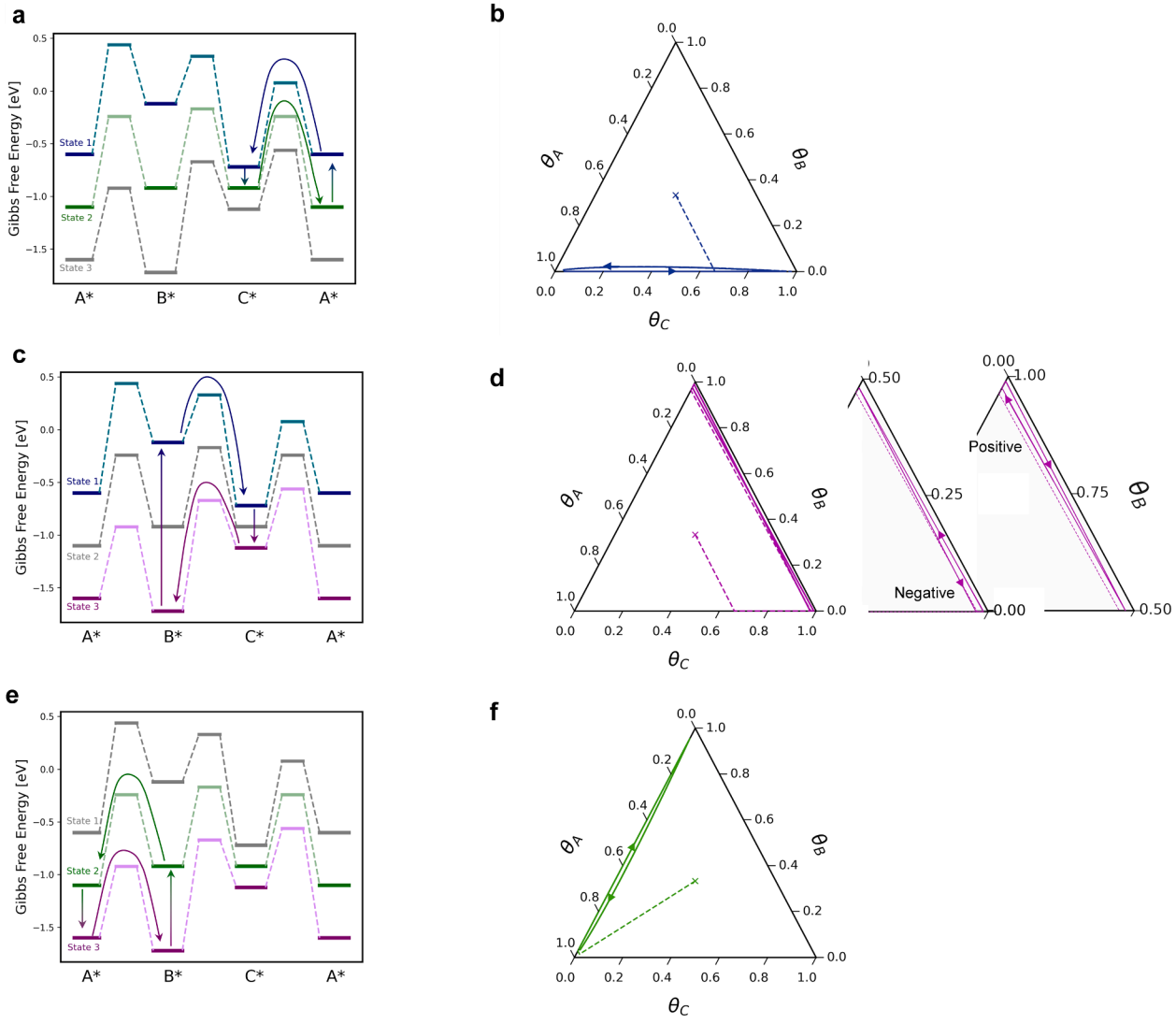

Fig. 7. Reduction of a 3 state system to 2 states. The data simulated in each panel is described by the same chemistry parameters: $\alpha_A = 0.6$, $\alpha_B = 0.5$, $\alpha_C = 0.4$, $\beta_A = 0.75$ eV, $\beta_B = 0.75$ eV, $\beta_C = 0.75$ eV, $\gamma_{B-A} = 1.6$, $\gamma_{C-A} = 0.4$, $\delta_{B-A} = 1.4$eV, $\delta_{C-A} = 0.8$eV. **(a)** Oscillation between states 1 and 2 yields a two state system with a minimum binding energy of $BE_A = 0.6$ eV and an oscillation amplitude of $\Delta\ BE_A = 0.5$ eV. **(b)** Application of a square waveform at a frequency of 3.3 Hz yields oscillation between A* and C*. Leakage from C* to B* in state 2 yields a negative loop turnover frequency of -0.14 s^{-1}. **(c)** Oscillation between states 1 and 3 yields a two state system with a minimum binding energy of $BE_A = 0.6$ eV and an oscillation amplitude of $\Delta\ BE_A = 1.0$ eV. **(d)** Application of a square waveform at a frequency of 3.3 Hz yields oscillation between B* and C*. **(e)** Oscillation between states 2 and 3 yields a two state system with a minimum binding energy of $BE_A = 1.1$ eV and an oscillation amplitude of $\Delta\ BE_A = 0.5$ eV. **(d)** Application of a square waveform at a frequency of 3.3 Hz yields oscillation between A* and B*. Leakage from B* to C* in state 2 yields a positive loop turnover frequency of 0.14 s^{-1}.

Oscillating only between catalyst states 1 and 3 promoted oscillation between C* and B* on the surface, as outlined in Fig. 7**c**. Switching from state 1 to 3 promoted the reverse direction as C* reacted to form B*, while switching from state 3 to 1 promoted the forward direction of B* to C*. This oscillation produced a negligible loop turnover frequency at steady state, revealing the lack of net molecular flow about the loop. In this system, leakage was observed at both the onset on state 1 and 3. The high coverage of B* on the surface as state 3 switched to state 1 allowed for a portion of the B* to react in the reverse direction to form A*, which reacted to C* at the onset of state 1. Then, at the onset of the switch from state 1 to state 3, this high coverage of C* allowed for leakage forward to A* which reacted to form B*. These two conditions of leakage promoted two sections of opposite loop turnover frequency at steady state, which canceled to yield a negligible loop turnover frequency. In Fig. 7**d**, this is evident through the figure-eight shape of the steady state limit cycle.

Oscillating only between catalyst state 2 and 3 promoted oscillation between A* and B* on the surface, as outlined in Fig. 7**e**. Switching from state 2 to 3 promoted the forward reaction for A* to B*, while switching from state 3 to 2 promoted the reverse. The leaky ratchet of state 2 was realized at the onset of state 2, when the coverage of B* was high, allowing for a small portion of B* to react forward, rather than backwards, to form C* which reacted further favorably to A*. This slight promotion of the forward loop is evident as the dynamic system has a loop turnover frequency of 0.14 s^{-1} and the clockwise direction of the limit cycle in Fig. 7**f**.

The assessment of two-state oscillations in Fig. 7 provides deeper understanding of the three-state oscillations of Fig. 6. As shown in Fig. 7, the selected two states of oscillation for each of the three state pairs provide a condition to oscillate back and forth between only two predominant surface species. Therefore, combining three catalytic states together indicates that the direction of loop turnover frequency can be pre-selected by ordering the three catalytic states based on the strongest binding surface species. In other words, molecules are continuously moved down a free energy gradient as the surface energy changes with oscillation with the aid of the ratchet structure of the free energy diagram.

3.6. *Importance and Implications of Catalytic Loop Turnover Frequency for Chemical Control*

The existence of non-zero loop turnover frequency under dynamic conditions poses both opportunities and challenges for the design and operation of programmable catalysts. Most reactions are comprised of multi-step chemistry, with complicated chemistries including parallel and series reaction networks. Consider the reaction network of Fig. 8**a**, where gaseous A(g) reacts on a surface to form gaseous D(g) and F(g). With four internal three-species reaction loops, the reaction pathways to form either D(g) or F(g) can include backwards progress provided loop turnover frequency of one of the loops is positive or negative. In the extreme case that loop III (B to E to C to E) became dominant, the entire catalyst surface would be covered in the three surface species B, E, and C, such that the overall reaction flux from A(g) to D(g) and F(g) was negligible. Energy input to the reacting surface would then be provided to oscillate the binding energies of adsorbates flowing in a loop, with only the generation of heat as the net outcome. This hypothetical dynamic system would have low reaction turnover efficiency, with molecules essentially trapped in the internal catalytic loop. Even more complicated issues arise when loops consist of four or more species (e.g., A* to B* to E* to C* to A*).

An alternative interpretation of catalytic loops is depicted in Fig. 8**b** that considers a surface reaction loop of three surface intermediates S1, S2, and S3. Interconversion of these intermediates consumes and produces gaseous species A(g) and B(g), such that the directionality of the overall reaction of A(g) to B(g) is determined by the catalytic surface loop. This type of catalytic reaction network could then be driven forward or backward dependent on the structure of the applied dynamic

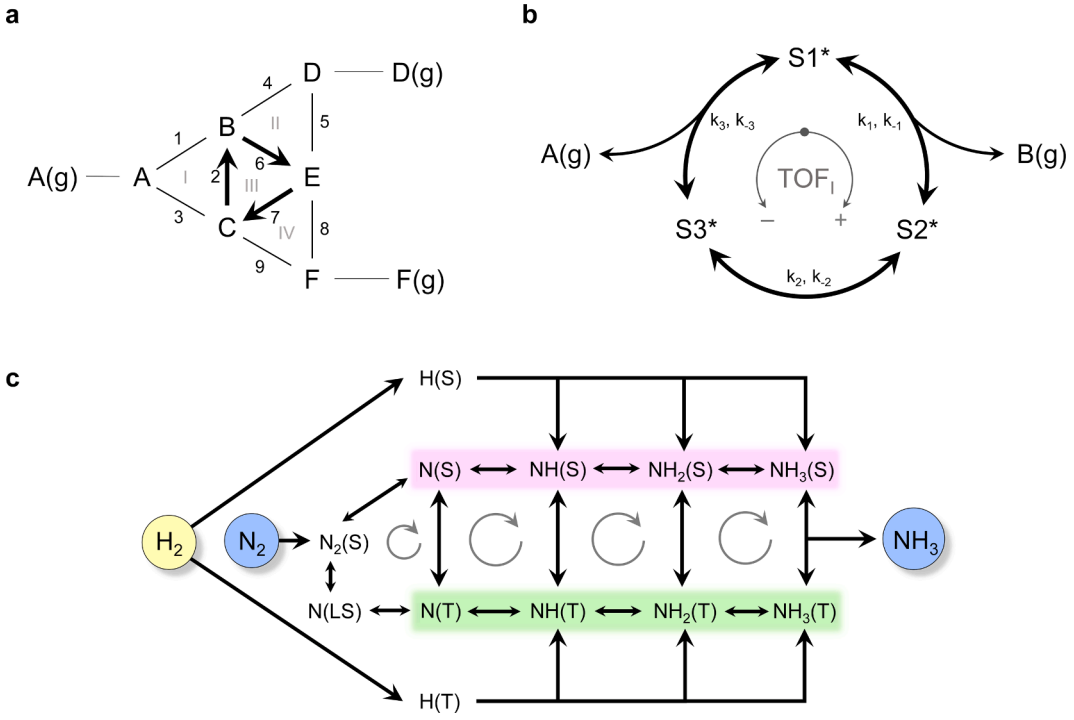

Fig. 8. Implications of Dynamic Catalytic Loops. (a) A reaction converting gaseous A to gaseous products D and F occurring through network of surface intermediates B, C, and E could exhibit reaction progression in a loop that limits the net overall reaction flux. **(b)** A surface reaction loop between surface species S1, S2, and S3 could reactor or form gaseous A and B, with the product being selected by the directionality of the reaction loop. (c) The synthesis of ammonia, NH_3, from hydrogen, H_2, and nitrogen, N_2, on ruthenium occurs on two active sites, the step (S) and terrace (T) sites, resulting in a series of four-species catalytic loops, in addition to multiple other loops within the reaction network.

program, as demonstrated in the case study of Fig. 6. The catalytic loop thereby serves as a catalytic surface pump pushing the overall reaction forward or backward with controllable external input.

These two examples of catalytic loops operating under dynamic surface modulation highlight the challenges and opportunities that exist in complex surface chemistry. Here, we have identified the existence of different types of loop behaviors including circumfluence (Figs. 2 and 3), two-species oscillations (Fig. 5), and dead-end single-species outcomes (Fig. 4) in addition to the potential benefits of applying more complex programs to control reaction loops (Fig. 6). This complexity will expand with combinations of reaction loops (Fig. 8), such that fundamental understanding and the ability to predict net flow of molecules in networks will ultimately dictate our ability to program surface chemistry for catalytic reaction control. One example of reaction loops in complex reaction networks is the synthesis of ammonia from hydrogen and nitrogen on ruthenium, as shown in Fig. 8**c**. This sequence of reactions dissociates N_2 and H_2 and then sequentially adds hydrogen to nitrogen to eventually produce NH_3. In this reaction, the same elementary step reaction occurs on both step (S) sites and terrace (T) sites, such that each step in the reaction sequence yields a four-species reaction loop. These types of multi-site loops (and many other types of loops) occur throughout heterogeneous catalysis due to the distribution of multiple site types (terrace, step, terrace, edge, corner) on bulk and particle catalysts, and should be expected to potentially exhibit loop turnover frequency under a limited set of conditions.

Future work aims to provide global understanding of catalytic loop turnover frequency in three species loops, larger 4 + species loops, and combinations of loops as they pertain to catalytic reaction networks. It remains to be determined if simple predictors that account for all of the chemical reaction parameters and applied program oscillation parameters can be identified to predetermine loop turnover frequency for any of these systems, including the simplest three-species catalytic loops.

4. Conclusions

The chemical behavior of a loop of three elementary surface reactions was evaluated by microkinetic modeling to assess the extent of flux of molecules around the loop (forward or backward) for a surface undergoing square or sinusoidal wave oscillations in electronic state. This system accounted for changes in surface energies via both linear scaling between each surface species (A*, B*, and C) and linear scaling of transition states (E_{a1}, E_{a2}, E_{a3}) for varying parameters of applied oscillation frequency, f, amplitude, ΔBE_A, oscillation energy lower bound, oscillation shape (square or sinusoidal wave), and initial surface conditions (θ_A°, θ_B°, and θ_C°). Parameter sets were identified to demonstrate three classes of behaviors for two-state dynamic programs including: (i) significant loop turnover frequency in excess of 1 s^{-1} in either clockwise or counterclockwise direction, (ii) oscillation of the surface between predominately two surface species with negligible overall loop turnover frequency, and (iii) termination of the reaction with a surface predominately covered in only one surface species. More complicated behavior was observed for dynamic programs consisting of three energy states, such that catalytic loop turnover frequency could be switched between positive (clockwise) and negative (counterclockwise) flux of molecules around the catalytic loop depending on the design of the applied program. The significant number of parameters associated with both the dynamic chemical surface reactions and the applied dynamic program prohibits a priori identification of a simple descriptor for predicting catalytic loop turnover frequency.

CRediT authorship contribution statement

Madeline A. Murphy: Formal analysis, Investigation, Methodology, Software, Visualization, Writing – original draft, Writing – review & editing. **Sallye R. Gathmann:** Conceptualization, Investigation, Methodology, Software, Writing – original draft, Writing – review & editing. **Christopher J. Bartel:** Data curation, Formal analysis, Software, Supervision. **Omar A. Abdelrahman:** Conceptualization, Writing – original draft, Writing – review & editing. **Paul J. Dauenhauer:** Conceptualization, Investigation, Supervision, Visualization, Writing – original draft, Writing – review & editing.

Declaration of competing interest

The authors declare the following financial interests/personal relationships which may be considered as potential competing interests: Paul Dauenhauer reports financial support was provided by US Department of Energy.

Data availability

Data is available via online database described in the supporting information

Acknowledgements

This work was supported as part of the Center for Programmable Energy Catalysis, an Energy Frontier Research Center funded by the U.S. Department of Energy, Office of Science, Basic Energy Sciences at the University of Minnesota under award #DE-SC0023464.

Appendix A. Supplementary material

Additional details including: Binding energies derivation, microkinetic model derivation, ODE solver comparison, code development and block logic diagrams, loop dynamic simulation Julia code, ternary plotting Python code, data repository (DRUM) access.

Supplementary data to this article can be found online at https://doi.org/10.1016/j.jcat.2024.115343.

References

[1] R. Aris, Mathematical aspects of chemical reaction, Ind. Eng. Chem. 61 (6) (1969) 17–29.
[2] S. Rangarajan, A. Bhan, P. Daoutidis, Language-oriented rule-based reaction network generation and analysis: description of RING, Comput. Chem. Eng. 45 (2012) 114–123, https://doi.org/10.1016/j.compchemeng.2012.06.008.
[3] N.K. Razdan, T.C. Lin, A. Bhan, Concepts relevant for the kinetic analysis of reversible reaction systems, Chem. Rev. 123 (6) (2023) 2950–3006, https://doi.org/10.1021/acs.chemrev.2c00510.
[4] R., W. G., L. Shizhong, J., D. P., G., V. D. Catalytic resonance of ammonia synthesis by simulated dynamic ruthenium crystal strain. Sci. Adv. 8 (4) (2022) eabl6576. 10.1126/sciadv.abl6576.
[5] A.H. Motagamwala, J.A. Dumesic, Microkinetic modeling: A tool for rational catalyst design, Chem. Rev. 121 (2) (2021) 1049–1076, https://doi.org/10.1021/acs.chemrev.0c00394.
[6] G.R. Wittreich, K. Alexopoulos, D.G. Vlachos, microkinetic modeling of surface catalysis, in: W. Andreoni, S. Yip, (Eds.), Handbook of Materials Modeling: Applications: Current and Emerging Materials, Springer International Publishing, Cham, 2020, pp 1377–1404. 10.1007/978-3-319-44680-6_5.
[7] L. de Oliveira, B. Campos, K. Herrera Delgado, S. Pitter, J. Sauer, Development of Consistent Kinetic Models Derived from a Microkinetic Model of the Methanol Synthesis, Ind. Eng. Chem. Res. 60 (42) (2021) 15074–15086, https://doi.org/10.1021/acs.iecr.1c02952.
[8] A.G. Fredrickson, Stochastic Triangular Reactions, Chem. Eng. Sci. 21 (8) (1966) 687–691, https://doi.org/10.1016/0009-2509(66)80018-0.
[9] L. Onsager, Reciprocal Relations in Irreversible Processes I. Phys. Rev. 37 (4) (1931) 405–426, https://doi.org/10.1103/PhysRev.37.405.
[10] I. Aprahamian, S.M. Goldup, Non-Equilibrium Steady States in Catalysis, Molecular Motors, and Supramolecular Materials: Why Networks and Language Matter, J. Am. Chem. Soc. (2023), https://doi.org/10.1021/jacs.2c12665.
[11] D.G. Blackmond, "If Pigs Could Fly" Chemistry: A Tutorial on the Principle of Microscopic Reversibility, Angew. Chemie - Int. Ed. 48 (15) (2009) 2648–2654, https://doi.org/10.1002/anie.200804566.
[12] T.C. Lin, N.K. Razdan, A. Bhan, Rates and Reversibilities in Interconnected Reaction Networks, ACS Catal. 12 (5) (2022) 3100–3110, https://doi.org/10.1021/acscatal.1c05344.
[13] W.P. Jencks, Catalysis in Chemistry and Enzymology, Vol. 47, McGraw-Hill Book Co, New York, NY, 1969. 10.1021/ed047pa860.2.

[14] R.D. Astumian, P.B. Chock, T.Y. Tsong, H.V. Westerhoff, Effects of Oscillations and Energy-Driven Fluctuations on the Dynamics of Enzyme Catalysis and Free-Energy Transduction, Phys. Rev. A 39 (12) (1989) 6416–6435, https://doi.org/10.1103/PhysRevA.39.6416.
[15] B. Robertson, R.D. Astumian, Michaelis-Menten Equation for an Enzyme in an Oscillating Electric Field, Biophys. J. 58 (4) (1990) 969–974, https://doi.org/10.1016/S0006-3495(90)82441-3.
[16] M. Shetty, A. Walton, S.R. Gathmann, M.A. Ardagh, J. Gopeesingh, J. Resasco, T. Birol, Q. Zhang, M. Tsapatsis, D.G. Vlachos, P. Christopher, C.D. Frisbie, O. A. Abdelrahman, P.J. Dauenhauer, The Catalytic Mechanics of Dynamic Surfaces: Stimulating Methods for Promoting Catalytic Resonance, ACS Catal. (2020) 12666–12695, https://doi.org/10.1021/acscatal.0c03336.
[17] J. Qi, J. Resasco, H. Robatjazi, I.B. Alvarez, O. Abdelrahman, P. Dauenhauer, P. Christopher, Dynamic Control of Elementary Step Energetics via Pulsed Illumination Enhances Photocatalysis on Metal Nanoparticles, ACS Energy Lett. 5 (11) (2020) 3518–3525, https://doi.org/10.1021/acsenergylett.0c01978.
[18] T.M. Onn, S.R. Gathmann, Y. Wang, R. Patel, S. Guo, H. Chen, J.K. Soeherman, P. Christopher, G. Rojas, K.A. Mkhoyan, M. Neurock, O.A. Abdelrahman, C. D. Frisbie, P.J. Dauenhauer, Alumina Graphene Catalytic Condenser for Programmable Solid Acids, JACS Au (2022), https://doi.org/10.1021/jacsau.2c00114.
[19] T.M. Onn, S.R. Gathmann, S. Guo, S.P.S. Solanki, A. Walton, B.J. Page, G. Rojas, M. Neurock, L.C. Grabow, K.A. Mkhoyan, O.A. Abdelrahman, C.D. Frisbie, P. J. Dauenhauer, Platinum Graphene Catalytic Condenser for Millisecond Programmable Metal Surfaces, J. Am. Chem. Soc. 144 (48) (2022) 22113–22127, https://doi.org/10.1021/jacs.2c09481.
[20] M.A. Ardagh, O.A. Abdelrahman, P.J. Dauenhauer, Principles of Dynamic Heterogeneous Catalysis: Surface Resonance and Turnover Frequency Response, ACS Catal. 9 (8) (2019) 6929–6937, https://doi.org/10.1021/acscatal.9b01606.
[21] S.R. Gathmann, M.A. Ardagh, P.J. Dauenhauer, Catalytic Resonance Theory: Negative Dynamic Surfaces for Programmable Catalysts, Chem Catal. (2022), https://doi.org/10.1016/j.checat.2021.12.006.
[22] Y.M. Psarellis, M.E. Kavousanakis, P.J. Dauenhauer, I.G. Kevrekidis, Writing the Programs of Programmable Catalysis, ACS Catal. 13 (11) (2023) 7457–7471, https://doi.org/10.1021/acscatal.3c00864.
[23] M.A. Ardagh, T. Birol, Q. Zhang, O.A. Abdelrahman, P.J. Dauenhauer, Catalytic Resonance Theory: SuperVolcanoes, Catalytic Molecular Pumps, and Oscillatory Steady State, Catal. Sci. Technol. 9 (18) (2019) 5058–5076, https://doi.org/10.1039/c9cy01543d.
[24] S. Amano, M. Esposito, E. Kreidt, D.A. Leigh, E. Penocchio, B.M.W. Roberts, Using Catalysis to Drive Chemistry Away from Equilibrium: Relating Kinetic Asymmetry, Power Strokes, and the Curtin-Hammett Principle in Brownian Ratchets, J. Am. Chem. Soc. 144 (44) (2022) 20153–20164, https://doi.org/10.1021/jacs.2c08723.
[25] R.D. Astumian, S. Mukherjee, A. Warshel, The Physics and Physical Chemistry of Molecular Machines, ChemPhysChem (2016) 1719–1741, https://doi.org/10.1002/cphc.201600184.
[26] G. Ragazzon, L.J. Prins, Energy Consumption in Chemical Fuel-Driven Self-Assembly, Nat. Nanotechnol. 13 (10) (2018) 882–889, https://doi.org/10.1038/s41565-018-0250-8.
[27] K. Das, L. Gabrielli, L.J. Prins, Chemically Fueled Self-Assembly in Biology and Chemistry, Angew. Chemie - Int. Ed. 60 (37) (2021) 20120–20143, https://doi.org/10.1002/anie.202100274.
[28] O.A. Abdelrahman, P.J. Dauenhauer, Energy Flows in Static and Programmable Catalysts, ACS Energy Lett. 8 (5) (2023) 2292–2299, https://doi.org/10.1021/acsenergylett.3c00522.
[29] K.-R. Oh, T.M. Onn, A. Walton, M.L. Odlyzko, C.D. Frisbie, P.J. Dauenhauer, Fabrication of Large Area Metal-on-Carbon Catalytic Condensers for Programmable Catalysis, ACS Appl. Mater. Interfaces Mater. (2023), https://doi.org/10.26434/chemrxiv-2023-bt10w.
[30] T.M. Onn, K.-R. Oh, D.Z. Adrahtas, J.K. Soeherman, J.A. Hopkins, C.D. Frisbie, P. J. Dauenhauer, Flexible and Extensive Platinum Ion Gel Condensers for Programmable Catalysis, ACS Nano (2023), https://doi.org/10.1021/acsnano.3c09815.
[31] J.E. Sutton, D.G. Vlachos, A Theoretical and Computational Analysis of Linear Free Energy Relations for the Estimation of Activation Energies, ACS Catal. 2 (8) (2012) 1624–1634, https://doi.org/10.1021/cs3003269.
[32] J. Greeley, Theoretical Heterogeneous Catalysis: Scaling Relationships and Computational Catalyst Design, Annu. Rev. Chem. Biomol. Eng. 7 (1) (2016) 605–635, https://doi.org/10.1146/annurev-chembioeng-080615-034413.
[33] Z.-J. Zhao, S. Liu, S. Zha, D. Cheng, F. Studt, G. Henkelman, J. Gong, Theory-Guided Design of Catalytic Materials Using Scaling Relationships and Reactivity Descriptors, Nat. Rev. Mater. 4 (12) (2019) 792–804, https://doi.org/10.1038/s41578-019-0152-x.